Electronic Supplementary Material (ESI) for Inorganic Chemistry Frontiers.

Supporting Information For

Redox-and Solvato-Magnetic Switching in a Tetrathiafulvalene-Based Triad Single-Molecule Magnet

Fabrice Pointillart,[a] Jessica Flores Gonzalez,[a] Vincent Montigaud,[a] Lorenzo Tesi,[b,c] Vladimir Cherkasov,[d] Boris Le Guennic,[a] Olivier Cador,[a] Lahcène Ouahab,[a] Roberta Sessoli[b] and Viacheslav Kuropatov*[d]*

[a] Univ Rennes, CNRS, ISCR (Institut des Sciences Chimiques de Rennes) - UMR 6226, F-35000 Rennes, France

[b] Dipartimento di Chimica "Ugo Schiff" & INSTM RU, Università degli Studi di Firenze, Via della Lastruccia 3-13, 50019 Sesto Fiorentino (Firenze), Italy

[c] Institute of Physical Chemistry, University of Stuttgart, Pfaffenwaldring 55, 70569, Stuttgart, Germany.

[d] G. A. Razuvaev Institute of Organometallic Chemistry of Russian Academy of Sciences, 603950, GSP-445, Trpinina str., 49, Nizhny Novgorod, Russia.

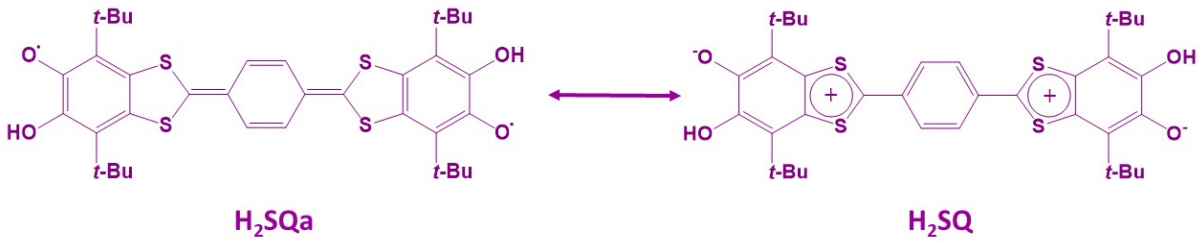

Scheme S1. Intramolecular electron transfer in **H_2SQ**.

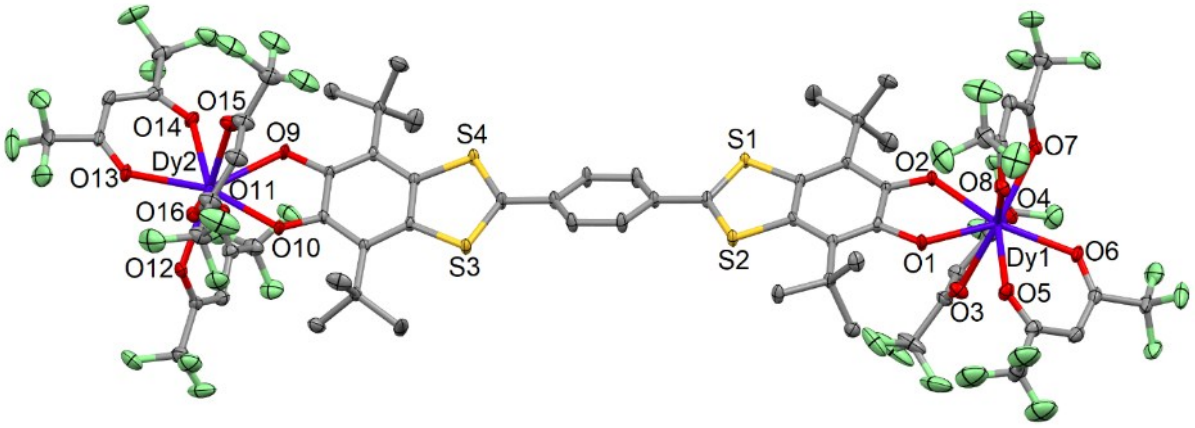

Figure S1. ORTEP view of the asymmetric unit in $[Dy_2(hfac)_6(\mathbf{H_2SQ})]\cdot CH_2Cl_2$ (**Dy_2H_2SQ**). Thermal ellipsoids are drawn at 30% probability. Hydrogen atoms and CH_2Cl_2 molecule of crystallisation are omitted for clarity.

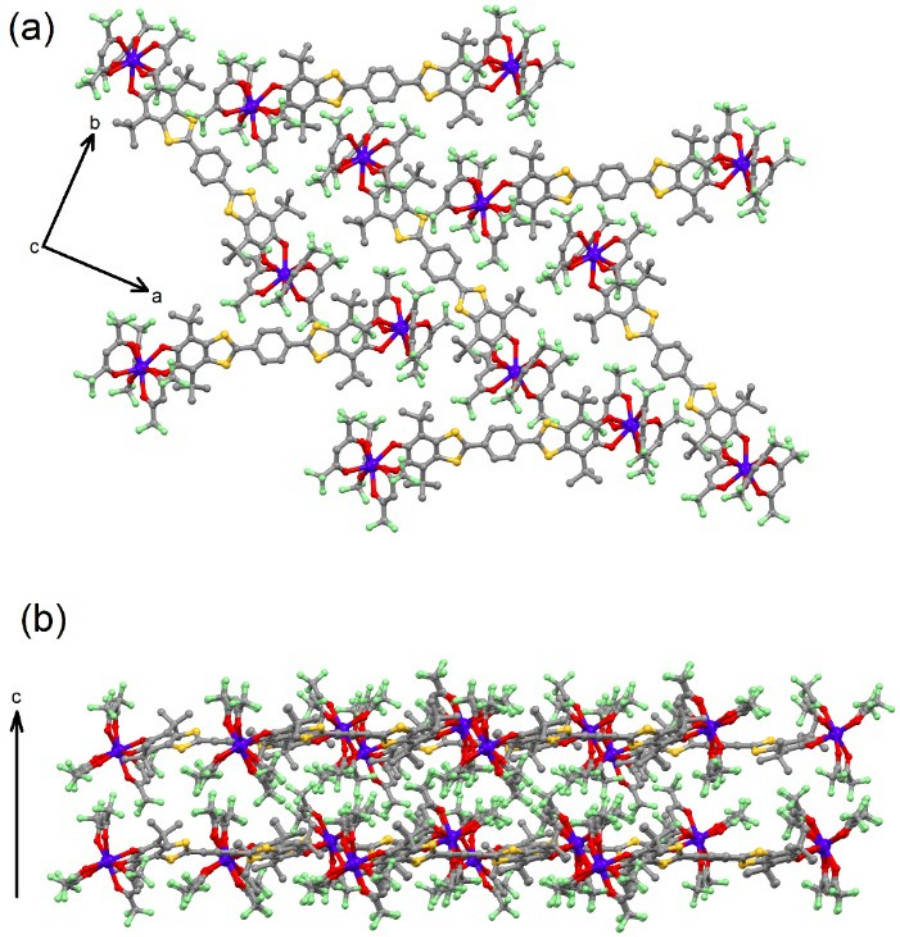

Figure S2. Crystal packing of **Dy_2H_2SQ** in the plan (110) (a) and along the c axis (b).

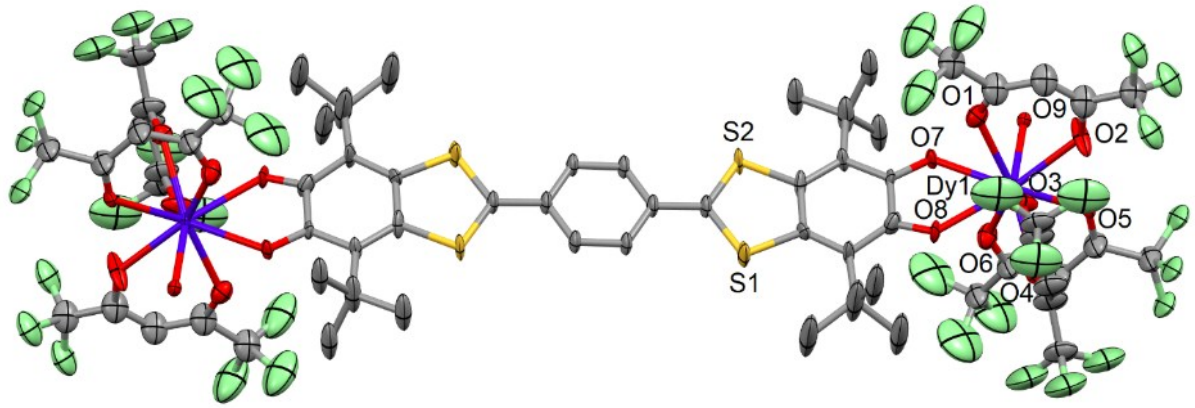

Figure S3. ORTEP view of the asymmetric unit in $[Dy(hfac)_3(\mathbf{Q})]_2$ (**Dy_2Q**). Thermal ellipsoids are drawn at 30% probability. Hydrogen atoms are omitted for clarity.

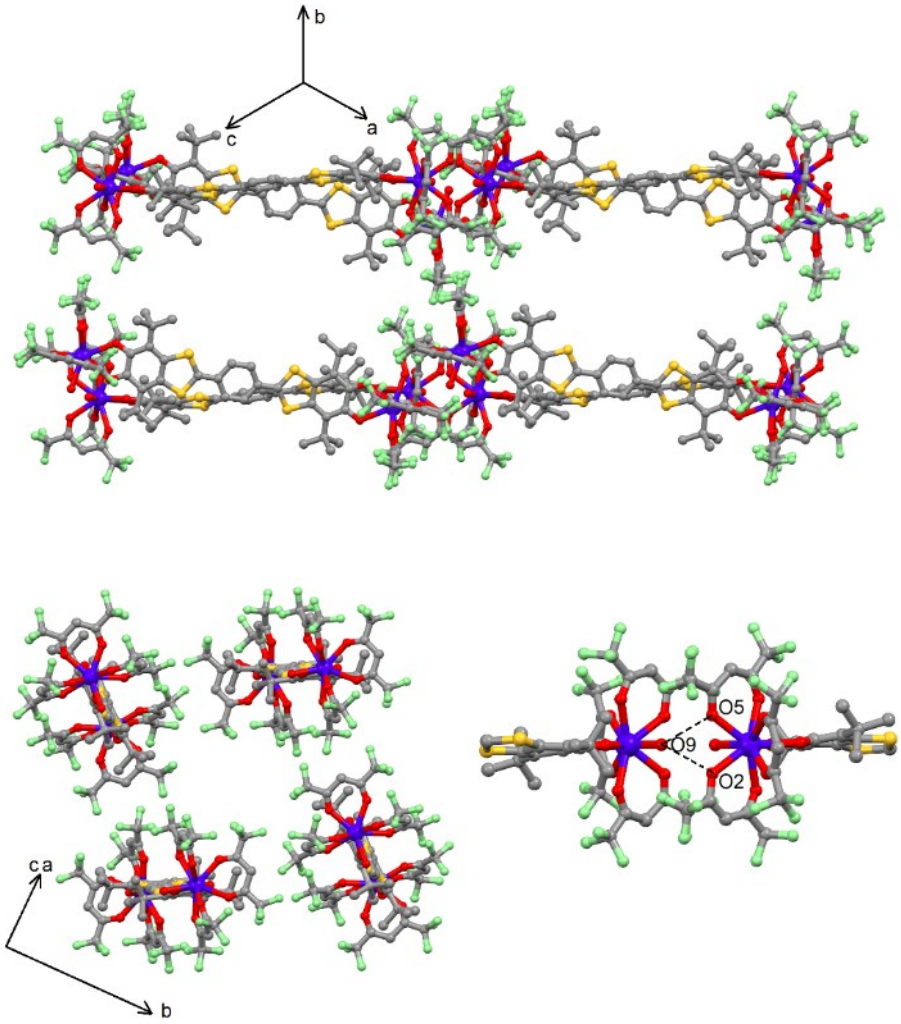

Figure S4. Crystal packing of **Dy_2Q** highlighting the formation of molecular chains through hydrogen bonds between the water molecule (O9) and oxygen atoms of the $hfac^-$ anions of the neighboring molecule (O2 and O5).

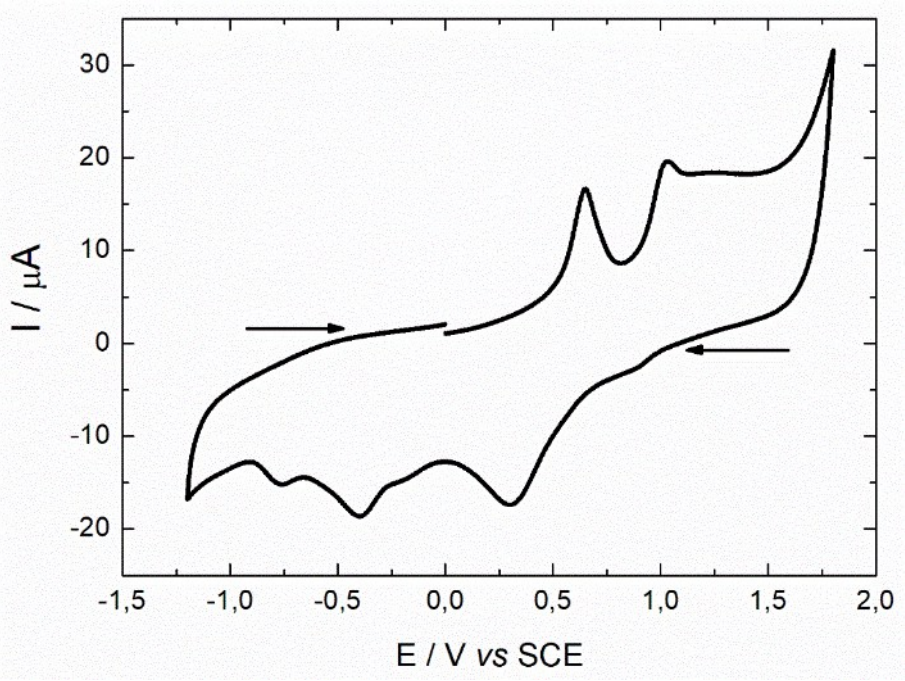

Figure S5. Cyclic voltammetry of **Dy_2H_2SQ** in CH_2Cl_2 at a scan rate of 100 $mV.s^{-1}$. The potentials were measured versus a saturated calomel electrode (SCE); Pt wire as the counter electrodes.

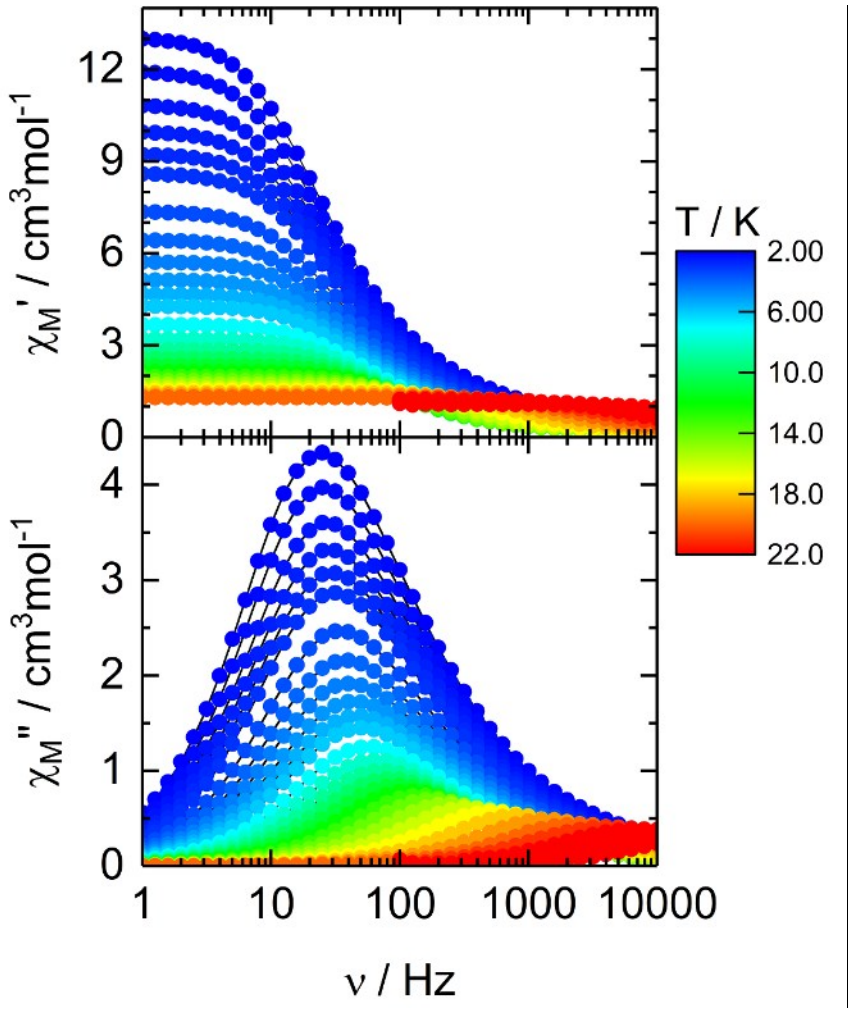

Figure S6. Frequency dependence of the in-phase (χ_M') and out-of-phase (χ_M'') components of the AC susceptibility for **Dy_2H_2SQ** at zero external DC magnetic field between 2 and 22 K.

AC magnetic susceptibility analysis

The frequency dependence of the AC susceptibility was reproduced with the extended Debye model leading to the following expressions:

$$\chi_M' = \chi_S + (\chi_T - \chi_S)\frac{1+(\omega\tau)^{1-\alpha}\sin\left(\alpha\frac{\pi}{2}\right)}{1+2(\omega\tau)^{1-\alpha}\sin\left(\alpha\frac{\pi}{2}\right)+(\omega\tau)^{2-2\alpha}}$$

$$\chi_M'' = (\chi_T - \chi_S)\frac{(\omega\tau)^{1-\alpha}\cos\left(\alpha\frac{\pi}{2}\right)}{1+2(\omega\tau)^{1-\alpha}\sin\left(\alpha\frac{\pi}{2}\right)+(\omega\tau)^{2-2\alpha}}$$

with χ_T the isothermal susceptibility, χ_S the adiabatic susceptibility, τ the relaxation time and α an empiric parameter which describes the distribution of the relaxation time. For SMM with only one relaxing object α is close to zero. The extended Debye model was applied to fit simultaneously the experimental variations of χ_M' and χ_M'' with the frequency ν of the oscillating field ($\omega = 2\pi\nu$). Typically, only the temperatures for which a maximum on the χ_M'' vs. ν curves is observed have been considered (see figure here below for an example). The best fitted parameters τ, α, χ_T, χ_S are listed in Table S3 to S5 with the coefficient of determination R^2.

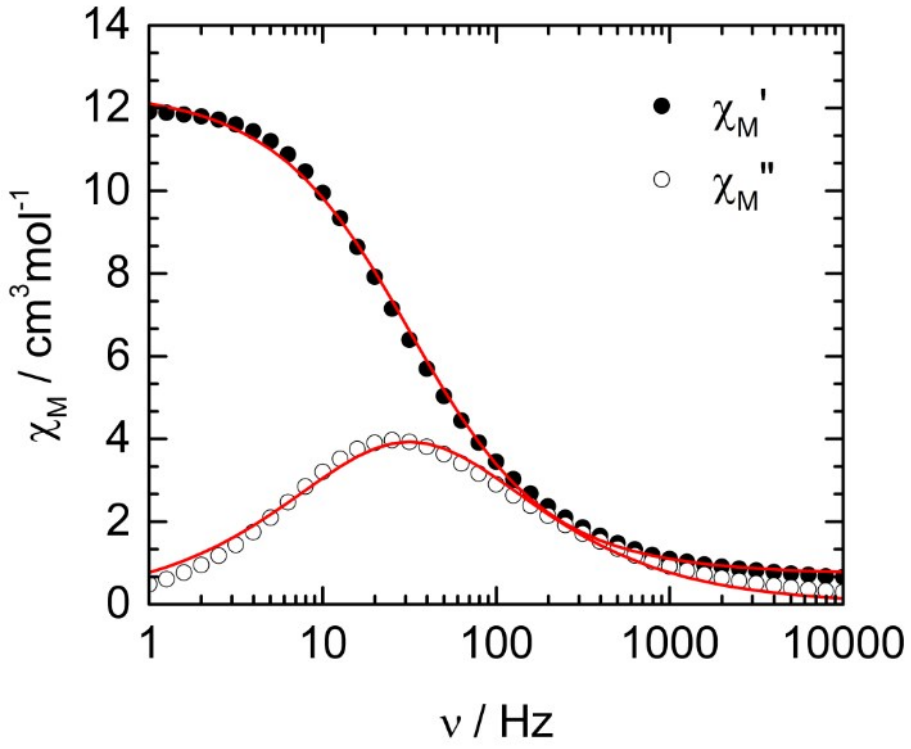

Figure S7. Frequency dependence of the in-phase (χ_M') and out-of-phase (χ_M'') components of the AC susceptibility measured on powder at 2.2 K at zero external DC magnetic field with the best fitted curves (red lines) for **Dy_2H_2SQ**.

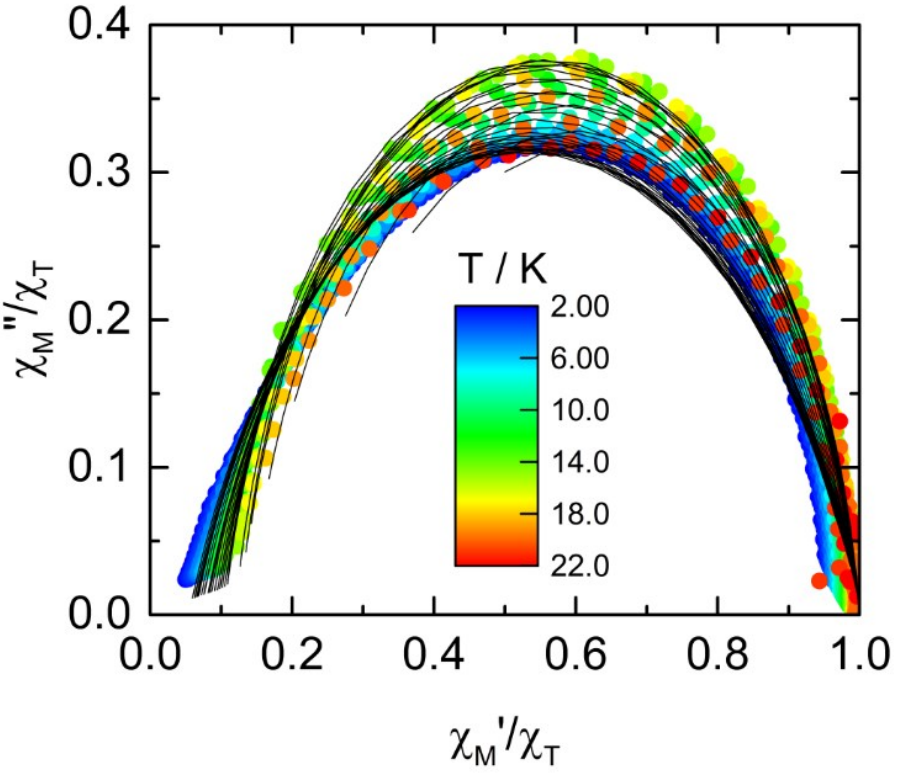

Figure S8. Normalized Cole-Cole plots for **Dy_2H_2SQ** at zero external DC magnetic field between 2 and 22 K.

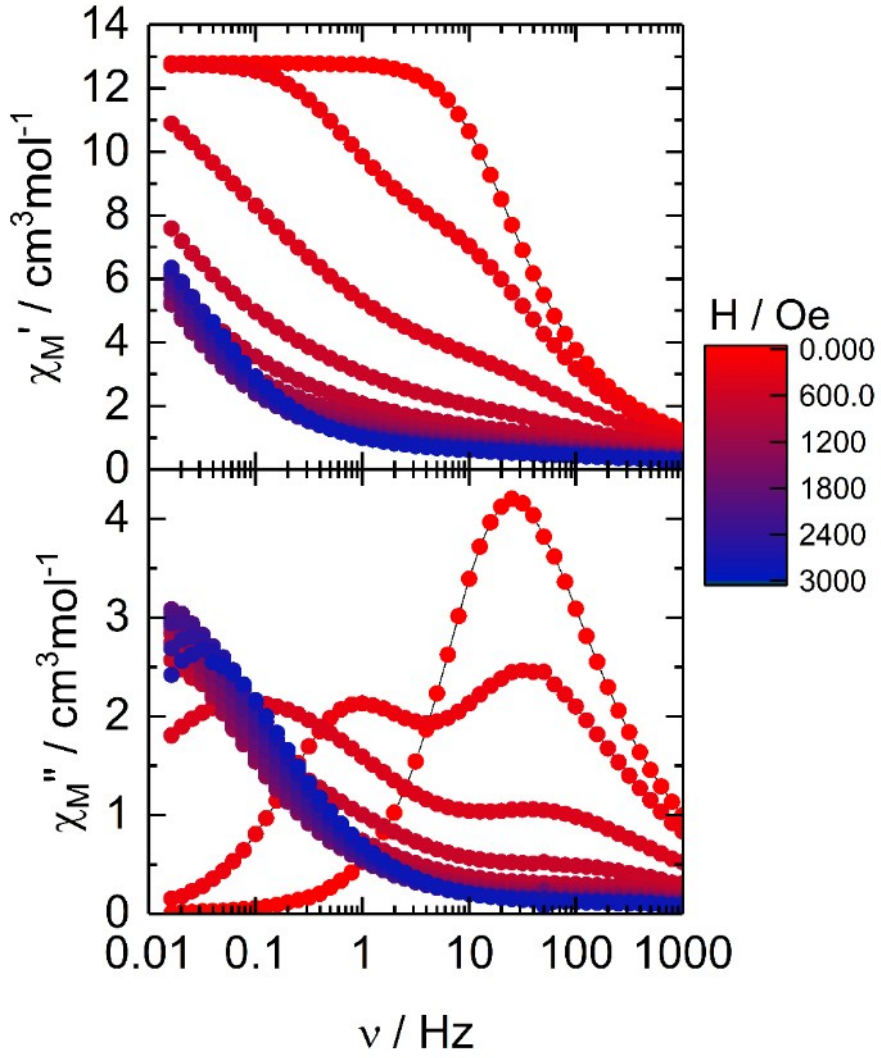

Figure S9 Frequency dependence of the in-phase (χ_M') and out-of-phase (χ_M'') components of the AC susceptibility for **Dy_2H_2SQ** between 0 and 3000 Oe external DC magnetic field at 2 K.

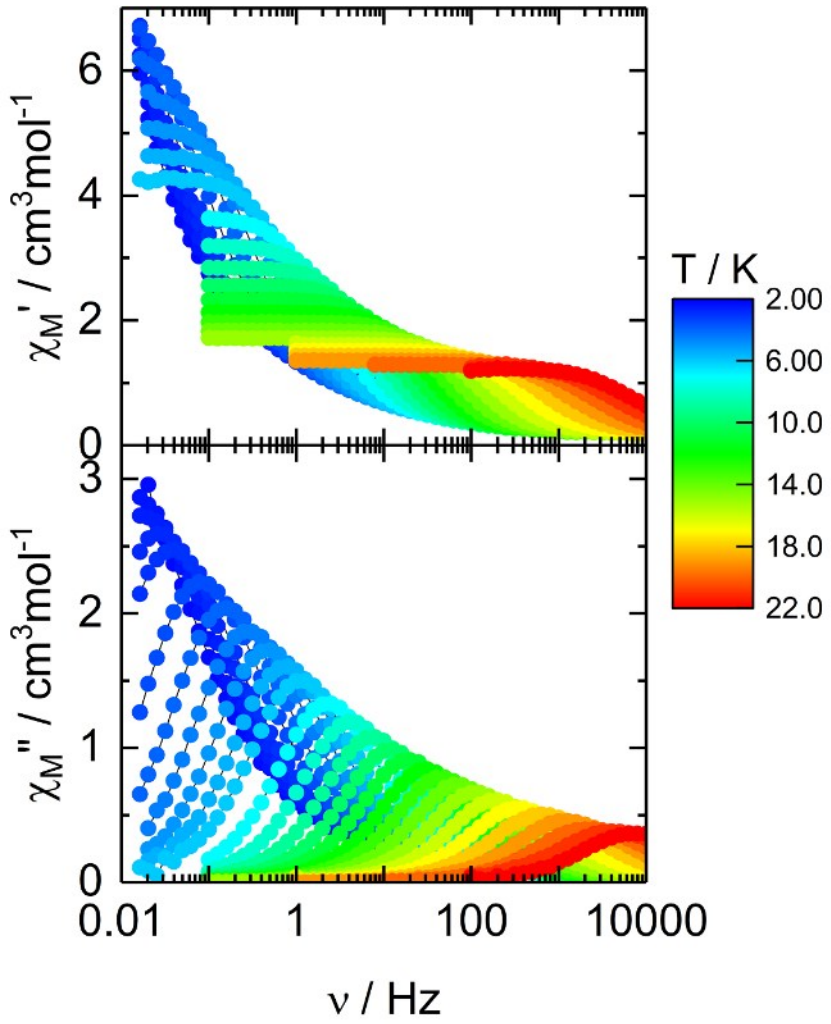

Figure S10. Frequency dependence of the in-phase (χ_M') and out-of-phase (χ_M'') components of the AC susceptibility for **Dy_2H_2SQ** at 1200 Oe external DC magnetic field between 2 and 22K.

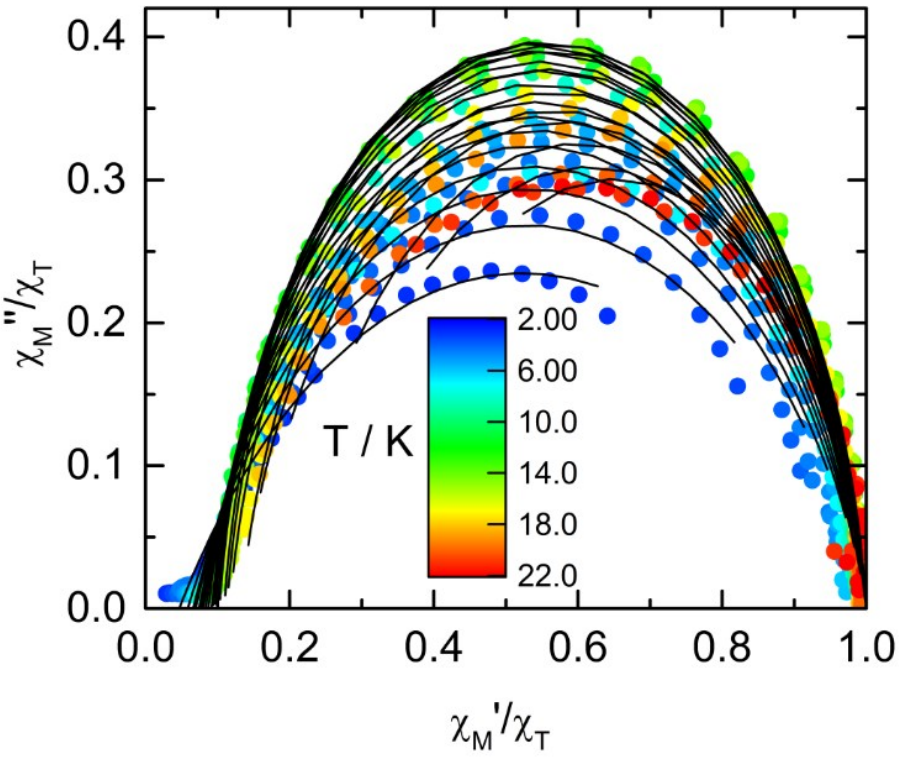

Figure S11. Normalized Cole-Cole plots for **Dy_2H_2SQ** at 1200 Oe external DC magnetic field between 2 and 22 K.

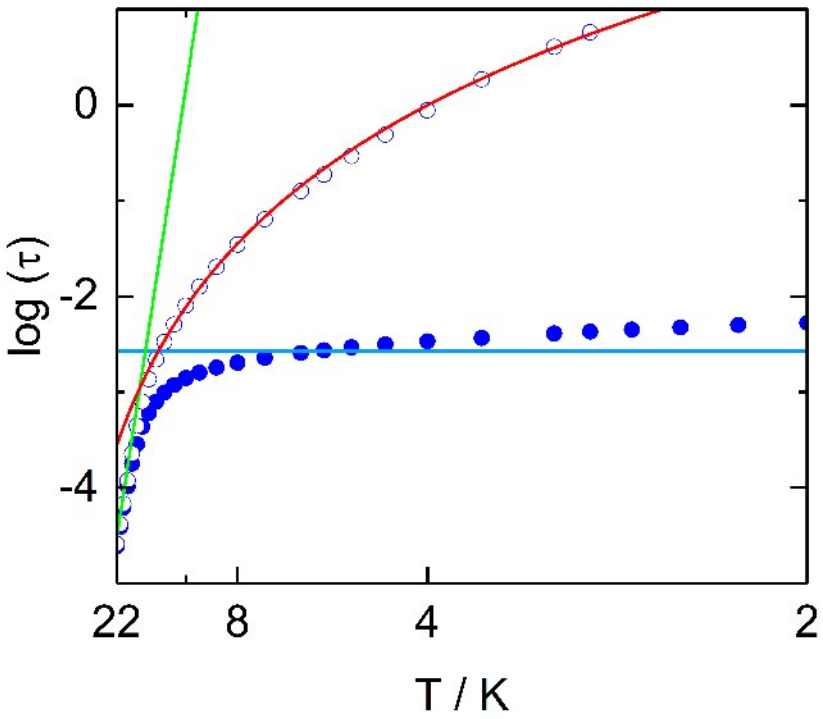

Figure S12. Arrhenius plots of the relaxation times at 0 Oe for **Dy_2H_2SQ** (blue disks) and at 1200 Oe for **Dy_2H_2SQ** (open blue circles). The colored dashed lines correspond to the main relaxation paths: Raman in red, Orbach in green and QTM in light blue.

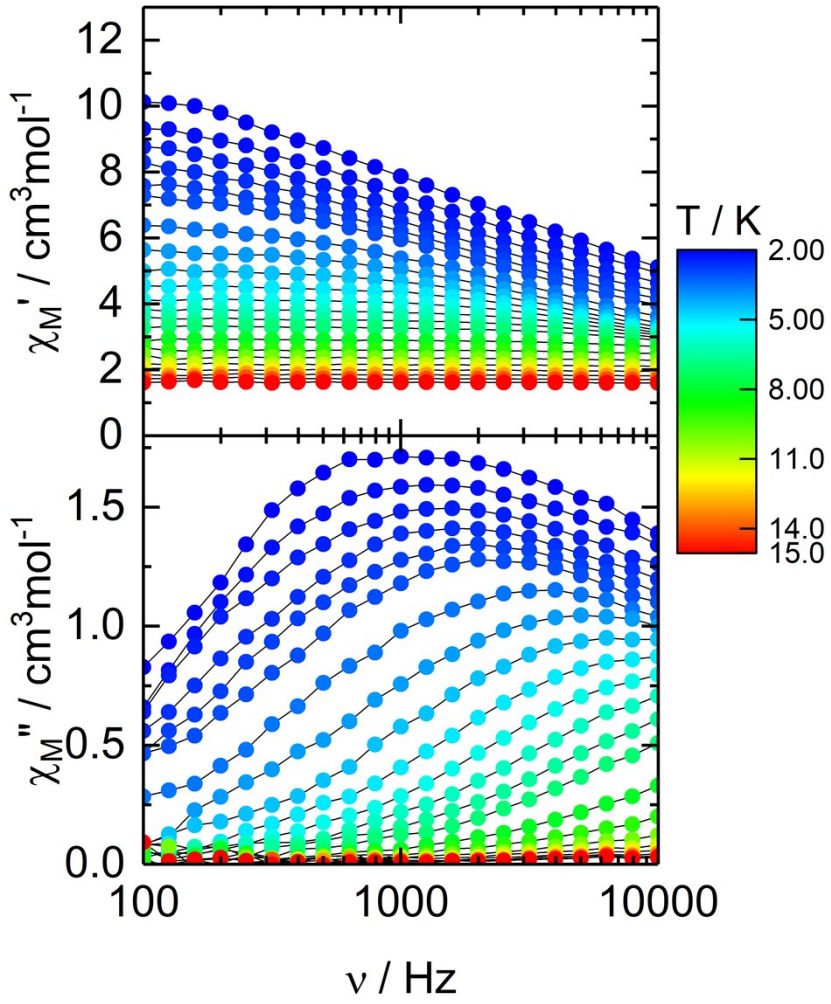

Figure S13. Frequency dependence of the in-phase (χ_M') and out-of-phase (χ_M'') components of the AC susceptibility for **Dy_2Q** in zero external DC magnetic field between 2 and 15 K.

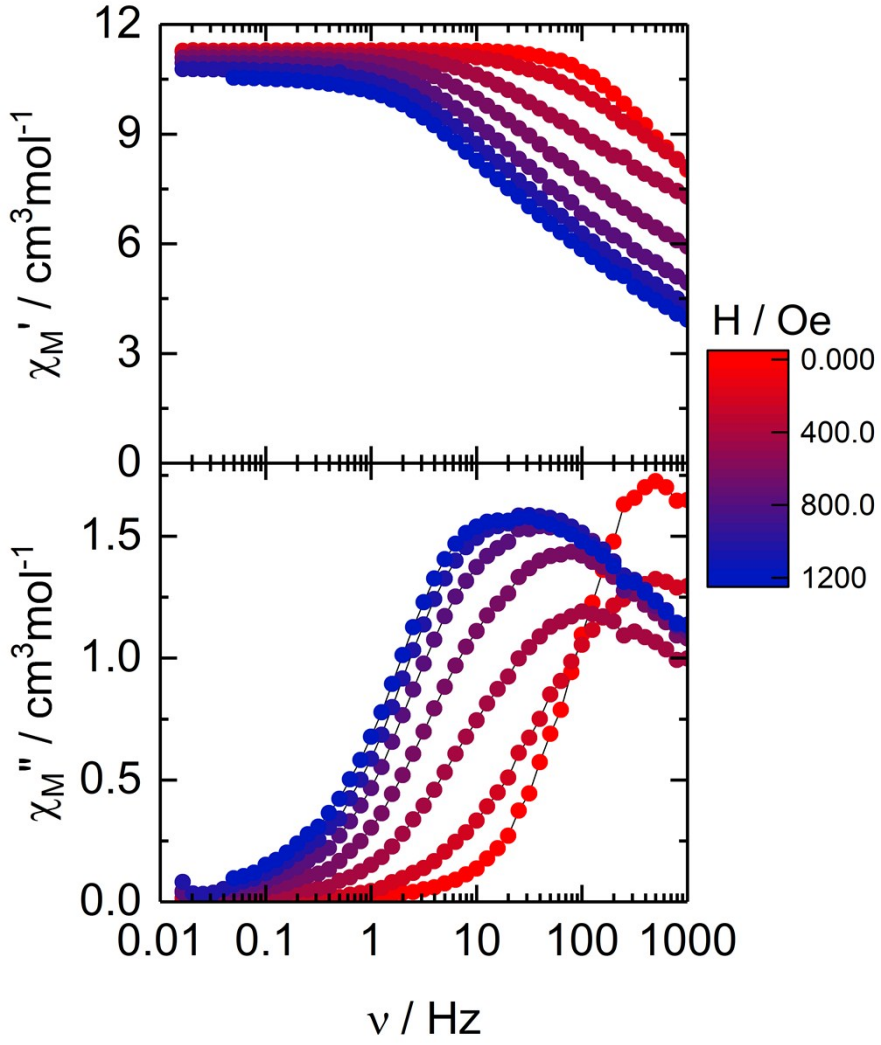

Figure S14. Frequency dependence of the in-phase (χ_M') and out-of-phase (χ_M'') components of the AC susceptibility for **Dy_2Q** between 0 and 3000 Oe at 2 K.

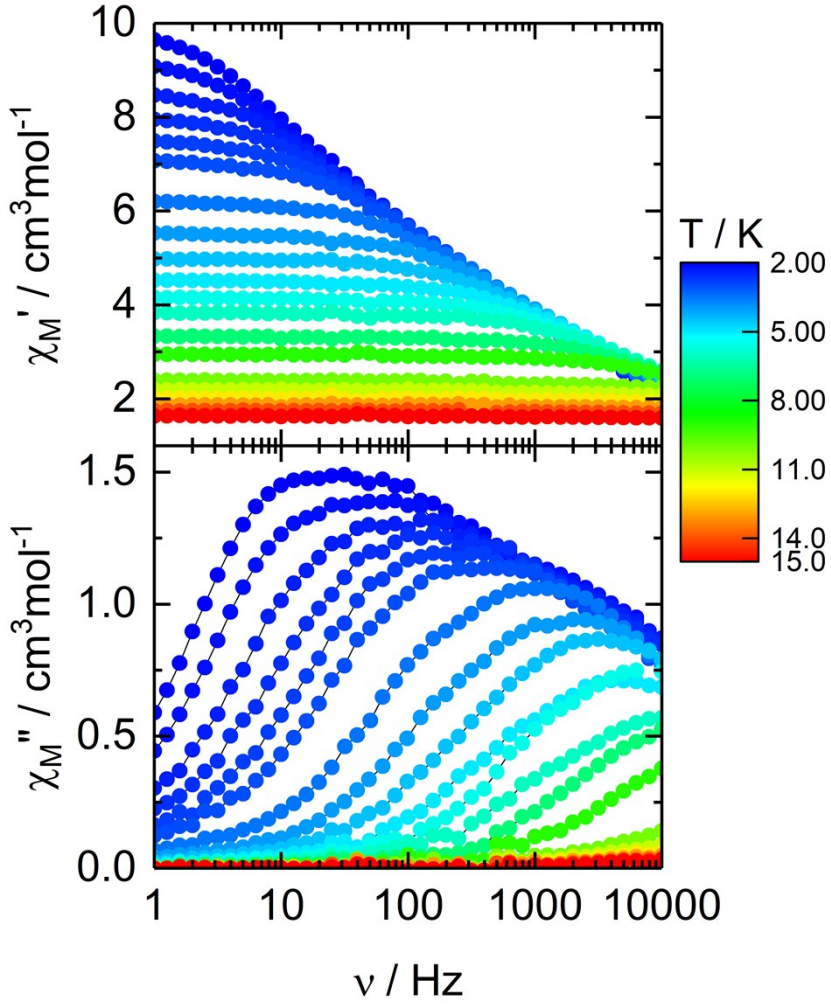

Figure S15. Frequency dependence of the in-phase (χ_M') and out-of-phase (χ_M'') components of the AC susceptibility for **Dy_2Q** at 1200 external DC magnetic field between 2 and 15 K.

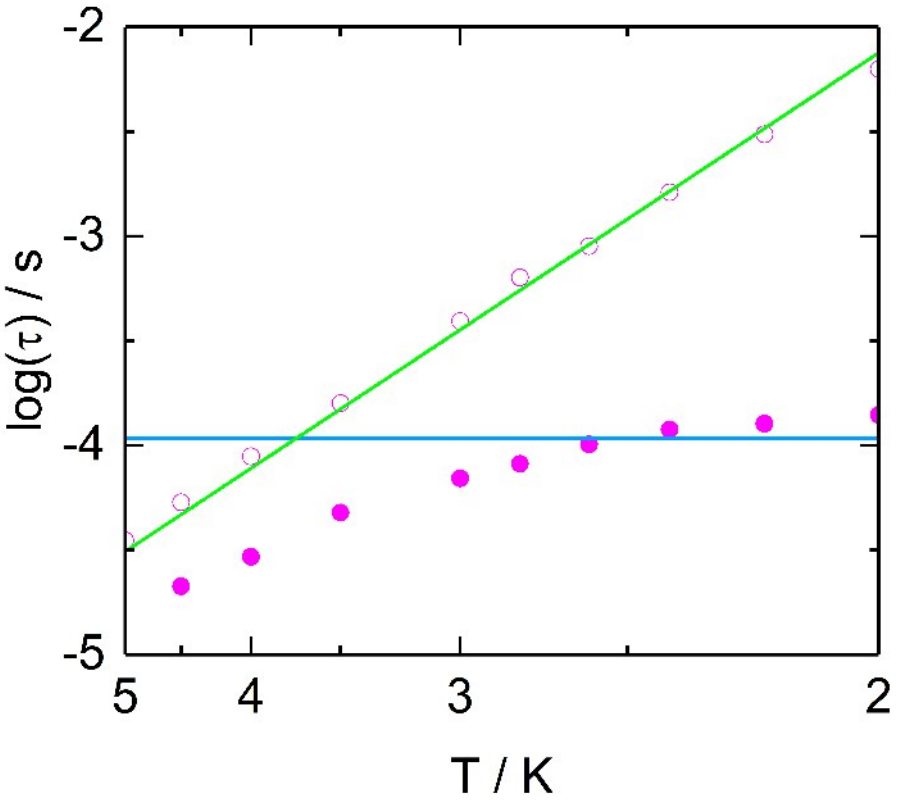

Figure S16. Arrhenius plots of the relaxation times at zero external DC magnetic field for **Dy_2Q** (pink disks) and at 1200 Oe external DC magnetic field for **Dy_2Q** (open pink circles). The colored dashed lines correspond to the different contributions to the main relaxation path: Orbach in green and QTM in light blue.

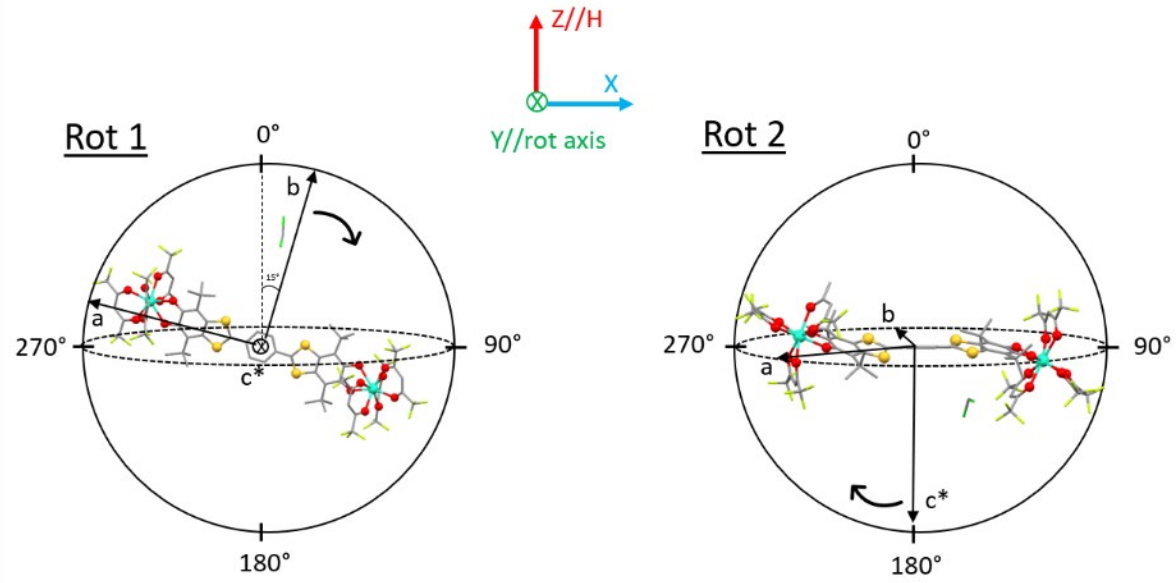

Figure S17. Graphic representation of the framework in which the two rotations (Rot 1 and Rot 2) were performed by CTM. As described in the main manuscript, XYZ is the laboratory framework, while *abc** is the crystallographic framework. The rotation can be easily visualized considering the *abc** reference frame rotating clockwise around the Y axis.

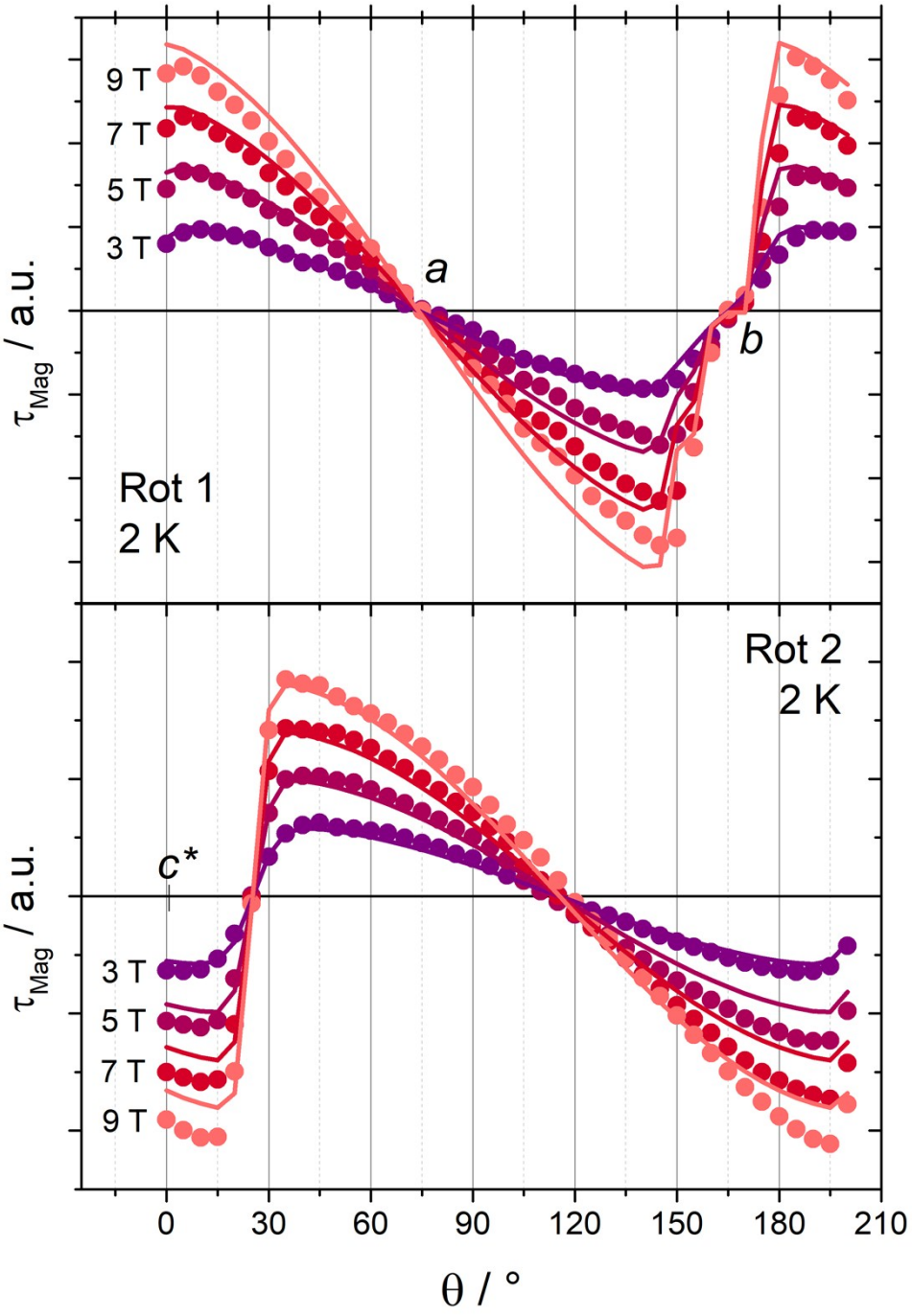

Figure S18. Experimental (dots) angular dependence of the magnetic torque for **Dy_2H_2SQ** in Rotation 1 (top) and Rotation 2 (bottom), measured at 2 K. The solid lines are the simulation curves obtained assuming the pseudo-spin ½ approximation and using the *g*-values found by *ab initio* calculations.

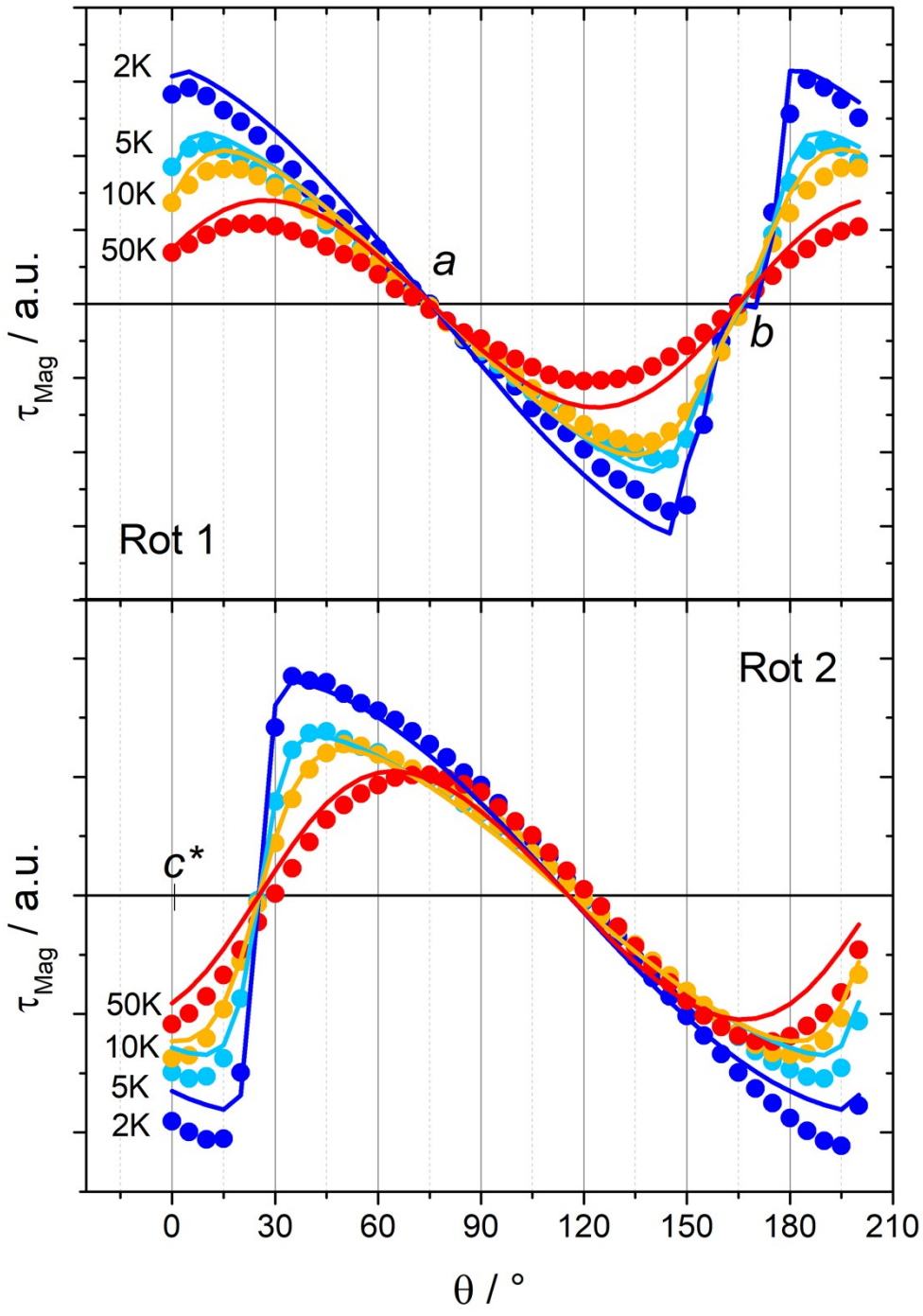

Figure S19. Experimental (dots) angular dependence of the magnetic torque for **Dy_2H_2SQ** in Rotation 1 (top) and Rotation 2 (bottom), measured at several temperature and magnetic field values (Rotation 1: 2 K and 9 T; 5 K and 7 T; 10 K and 7 T; 50 K and 9 T; Rotation 2: 2 K and 9 T; 5 K and 7 T; 10 K and 7 T; 50 K and 10 T). The solid lines are the simulation curves obtained using the *ab initio* calculated parameters relative to the full Hamiltonian model.

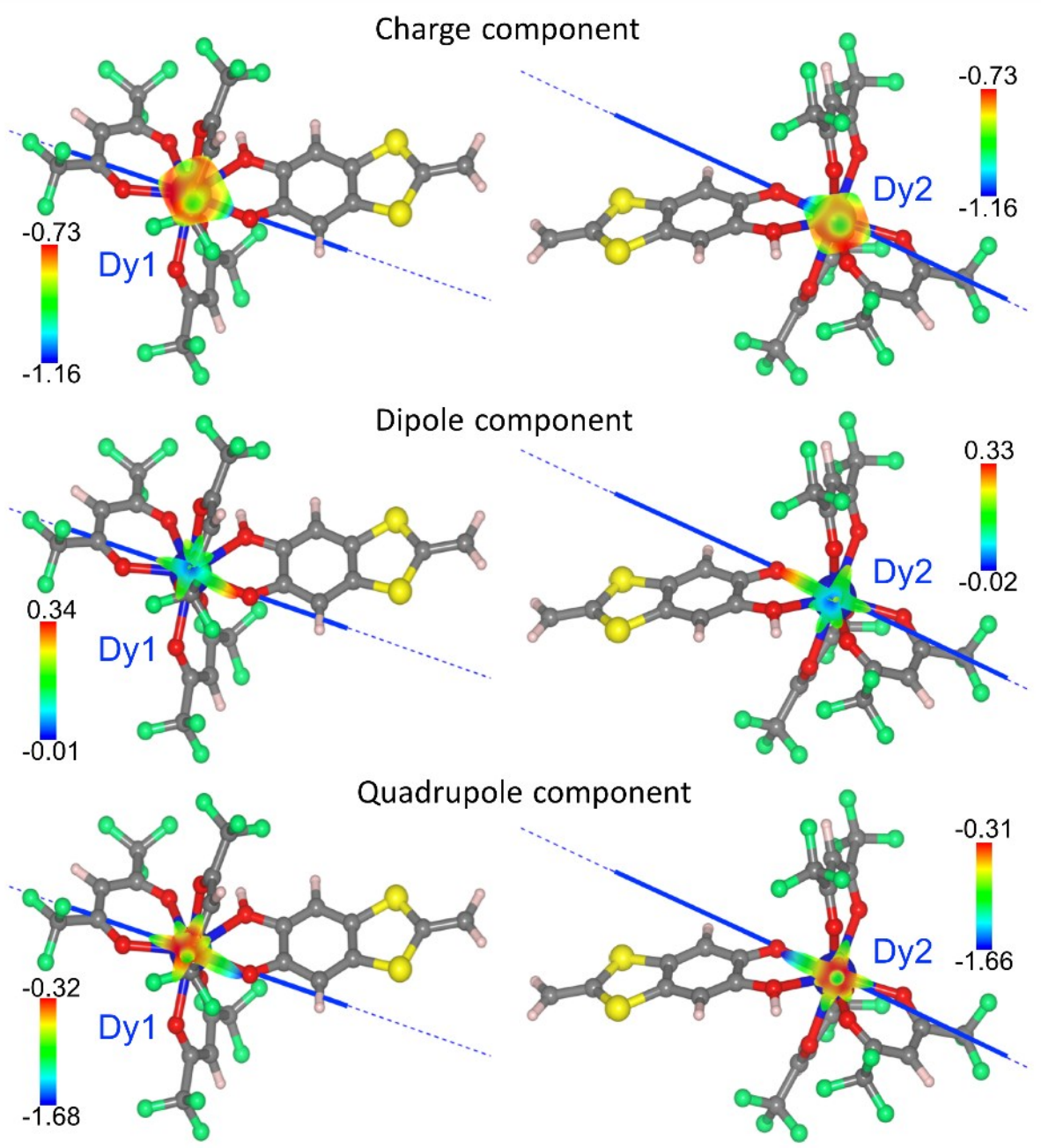

Figure S20. Decomposition of the molecular electrostatic potential into the charge (a), dipolar (b) and quadrupolar (c) components and projected on one of the Dy^{III} centers of **$Dy_2H_2SQ^m$.**

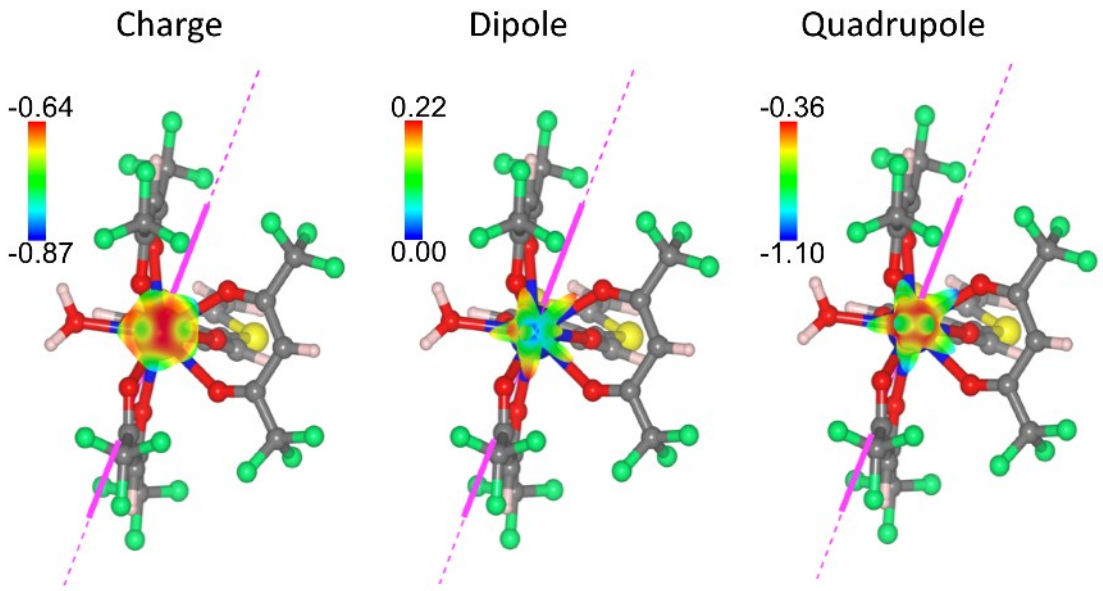

Figure S21. Decomposition of the molecular electrostatic potential into the charge (a), dipolar (b) and quadrupolar (c) components and projected on one of the Dy^{III} centers of $\mathbf{Dy_2Q^{mw}}$.

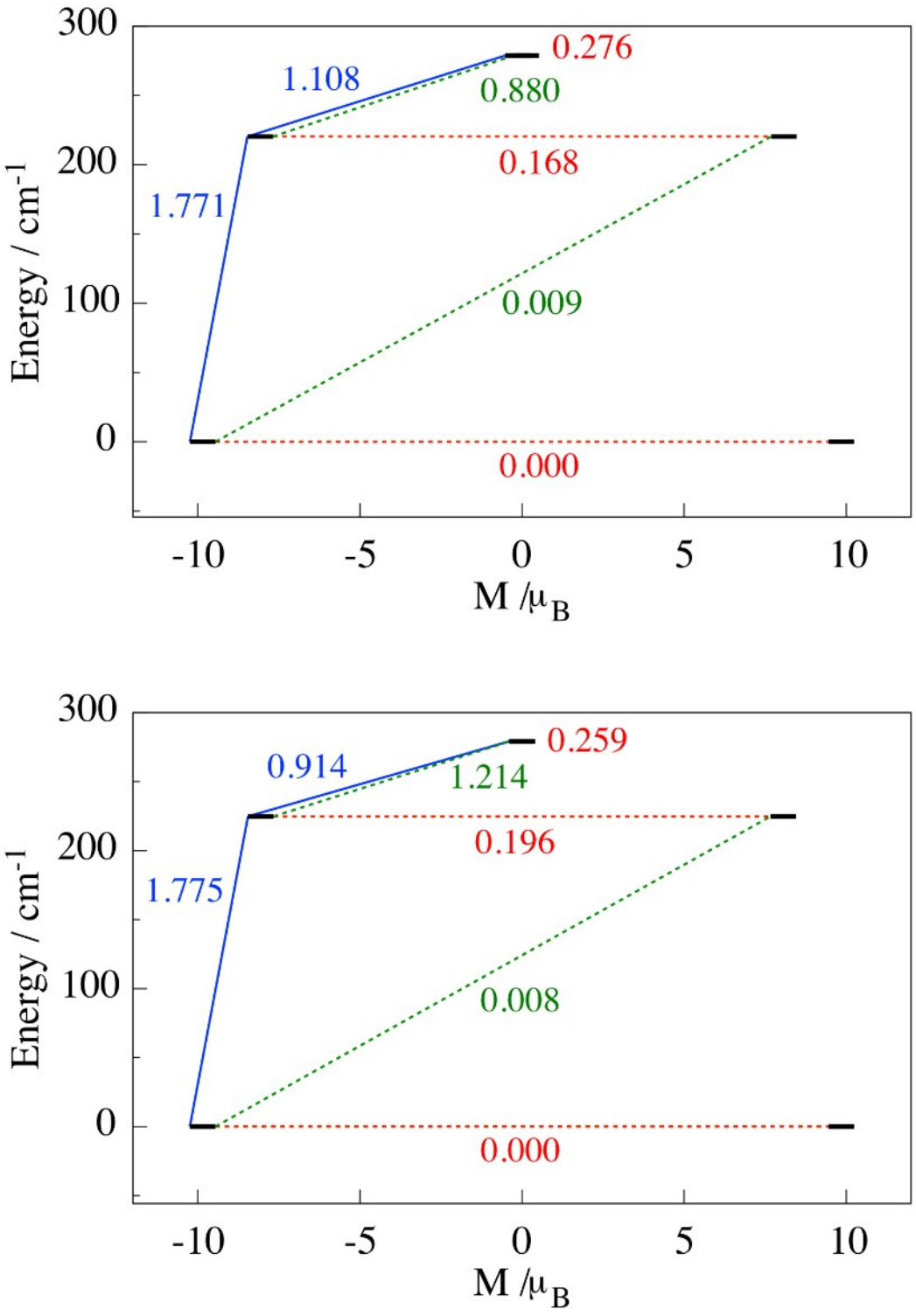

Figure S22. Single-ion relaxation pathways of **$Dy_2H_2SQ^m$** for each Dy^{III} centers, Dy1 (top) and Dy2 (bottom). Black lines are Kramers doublets as a function of computed magnetic moment, red lines are QTM/TA-QTM pathways, blue lines correspond to vertical excitation and green lines are Orbach relaxation pathways. The mean absolute values for the corresponding matrix element of transition magnetic dipole moment are represented with the numbers along the lines.

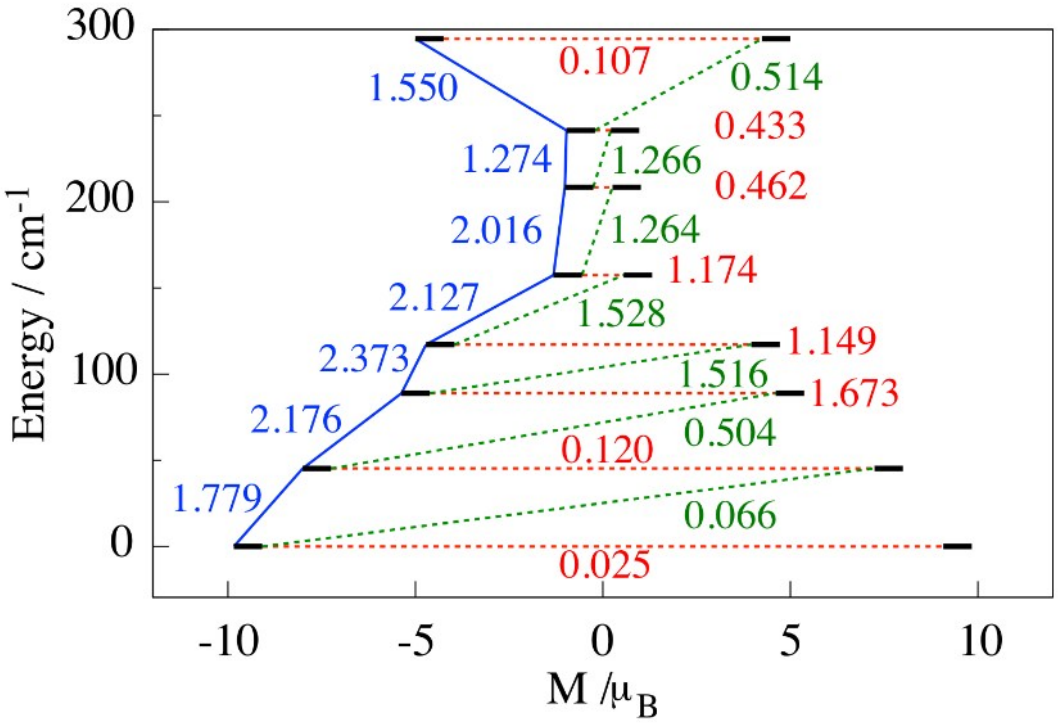

Figure S23. Single-ion relaxation pathways of **Dy_2Q^{mw}**. Black lines are Kramers doublets as a function of computed magnetic moment, red lines are QTM/TA-QTM pathways, blue lines correspond to vertical excitation and green lines are Orbach relaxation pathways. The mean absolute values for the corresponding matrix element of transition magnetic dipole moment are represented with the numbers along the lines.

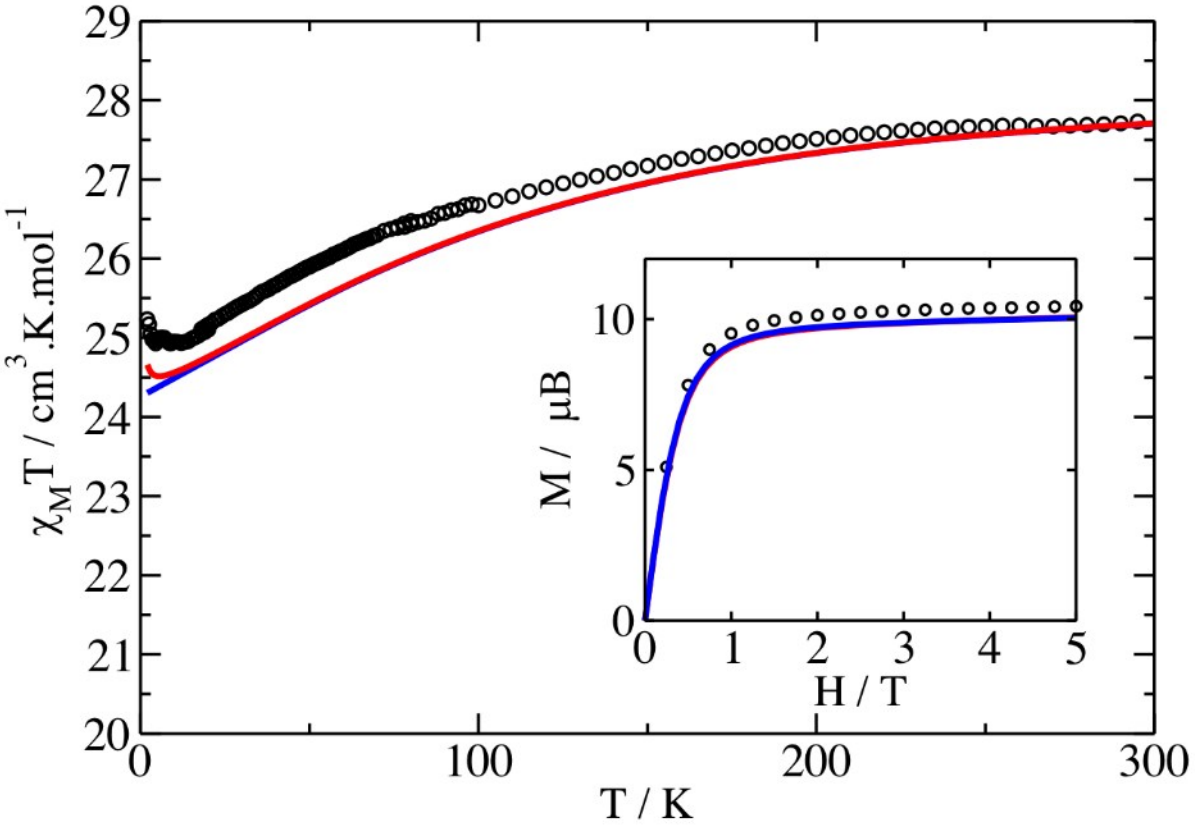

Figure S24. Thermal evolution of the magnetic susceptibility and field variation of the magnetization at 2K (inset) for **Dy_2H_2SQ**. The experimental data are represented as black dots while computed values with and without considering dipolar magnetic interactions are represented as red and blue curves, respectively.

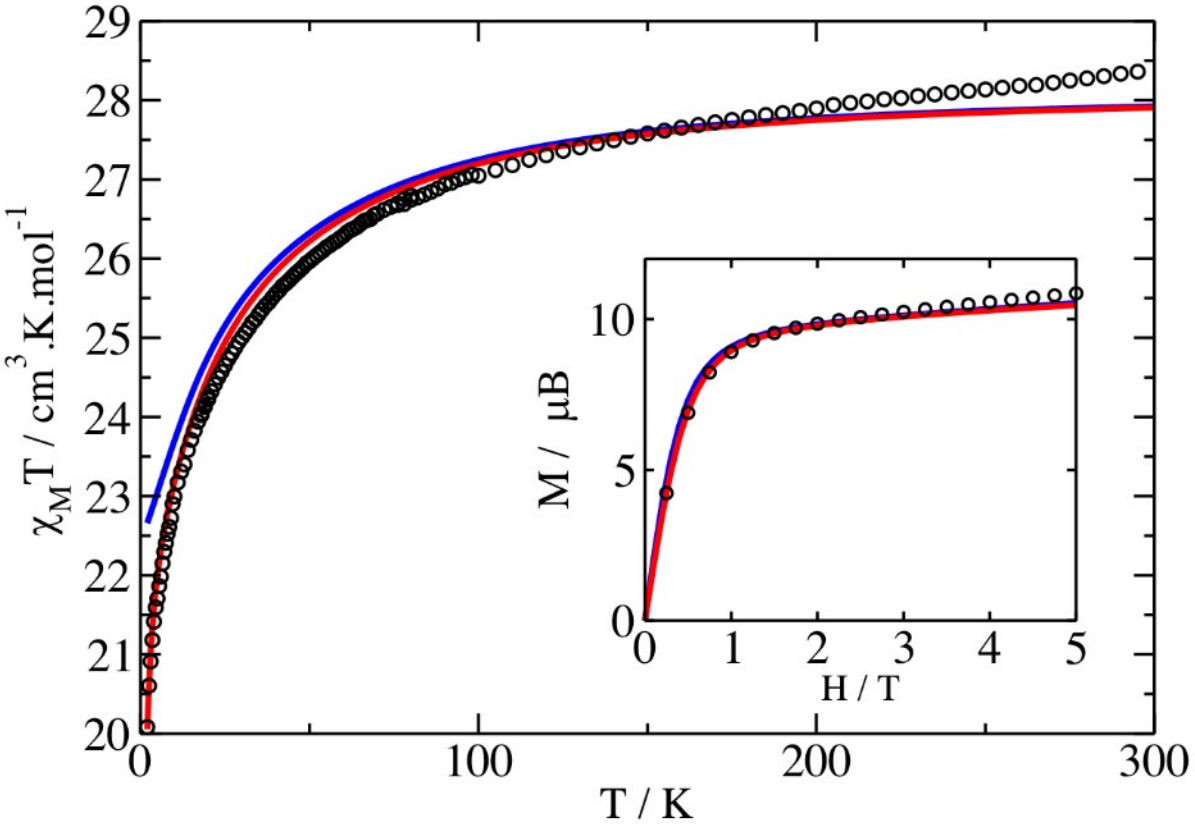

Figure S25. Thermal evolution of the magnetic susceptibility and field variation of the magnetization at 2K (inset) for **Dy_2Q**. The experimental data are represented as black dots lines while computed values with and without considering dipolar magnetic interactions J_1 are represented as red and blue curves, respectively.

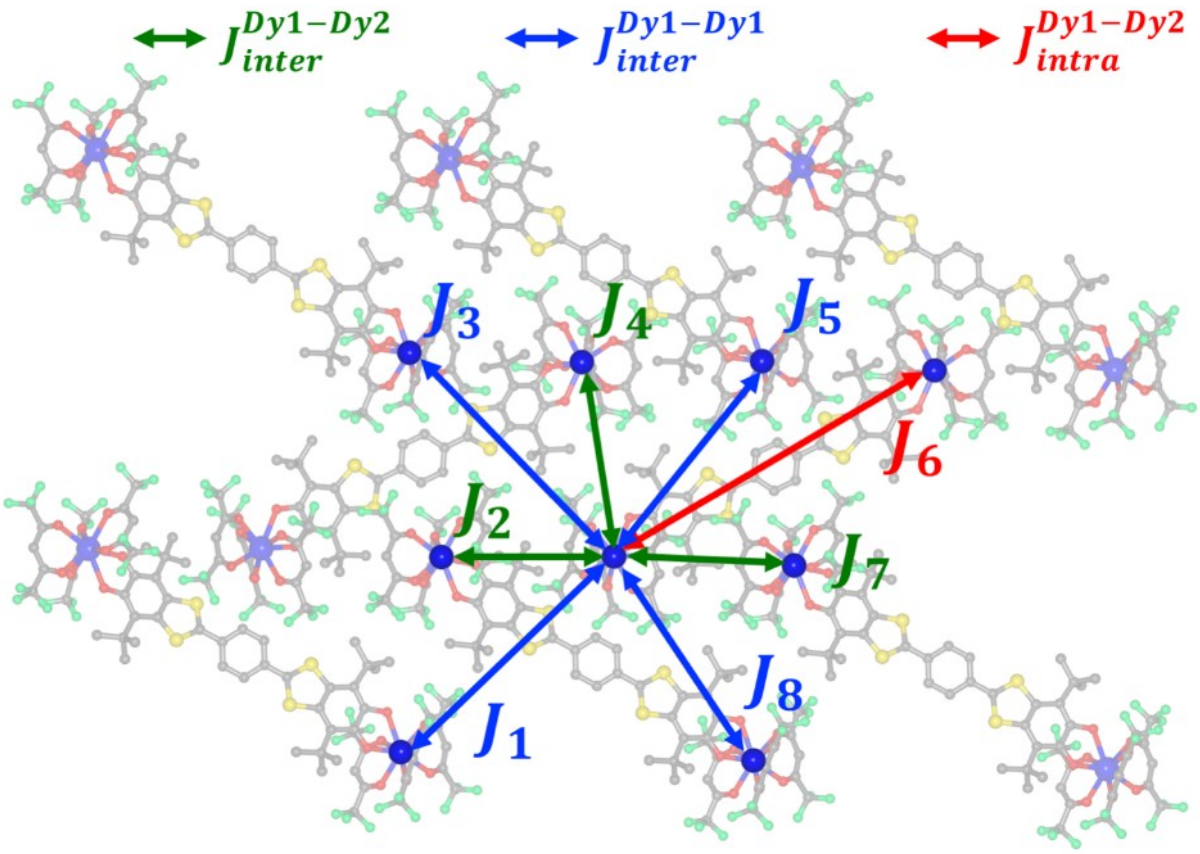

Figure S26. Representation of the dipolar interactions considered for **Dy_2H_2SQ**.

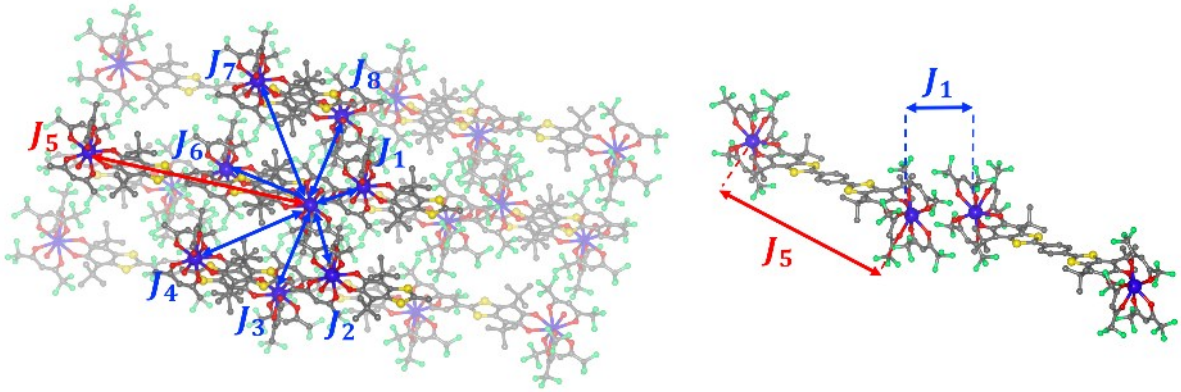

Figure S27. Representation of the intermolecular (blue arrows) and intramolecular (red arrow) dipolar interactions considered for **Dy_2SQ**.

Table S1. Crystallographic data for **Dy_2H_2SQ** and **Dy_2Q**.

Compounds	$[Dy_2(hfac)_6(\mathbf{H_2SQ})]\cdot CH_2Cl_2$ (**Dy_2H_2SQ**)	$[Dy(hfac)_3(\mathbf{Q})]_2$ (**Dy_2Q**)
Formula	$C_{67}H_{50}Cl_2Dy_2F_{36}O_{16}S_4$	$C_{66}H_{46}Dy_2F_{36}O_{18}S_4$
M / g.mol^{-1}	2317.5	2264.3
Crystal system	Monoclinic	Monoclinic
Space group	$P2_1/c$ (N°14)	$P2_1/n$
Cell parameters	a = 20.323(2) Å b = 22.995(3) Å c = 18.325(2) Å β = 94.943(4)°	a = 14.1076(14) Å b = 21.119(2) Å c = 17.2468(18) Å β = 112.037(3)°
Volume / Å^3	8531.8(17)	4763.0(8)
Cell formula units	4	4
T / K	150 (2)	150 (2)
Diffraction reflection	$5.91 \leq 2\theta \leq 54.97$	$6.09 \leq 2\theta \leq 54.97$
ρ_{calc}, g.cm^{-3}	1.806	1.579
μ, mm^{-1}	2.038	1.770
Number of reflections	80378	47086
Independent reflections	19494	10889
$Fo^2 > 2\sigma(Fo)^2$	14811	6473
Number of variables	1120	848
R_{int}, R_1, wR_2	0.0407, 0.0475, 0.1175	0.1237, 0.1405, 0.3424

Table S2. The three closest solutions of the SHAPE analysis for **Dy_2H_2SQ** and **Dy_2Q** compounds.

Dy_2H_2SQ		**Dy_2Q**
Dy1	*Dy2*	
Triangular dodecahedron (D_{2d}) 0.618	Triangular dodecahedron (D_{2d}) 0.652	Spherical capped square antiprism (C_{4v}) 0.178
Biaugmented trigonal prism (C_{2v}) 2.220	Biaugmented trigonal prism (C_{2v}) 1.682	Spherical tricapped trigonal prism (D_{3h}) 0.761
Snub diphenoid J84 (D_{2d}) 2.575	Square antiprism (D_{4d}) 2.386	Muffin (C_s) 0.836

Table S3. Best fitted parameters (χ_T, χ_S, τ and α) with the extended Debye model for compound **Dy_2H_2SQ** at 0 Oe in the temperature range 2-22 K.

T / K	χ_T / cm^3 mol^{-1}	χ_S / cm^3 mol^{-1}	α	τ / s	R^2
2	13.66292	0.74684	0.25421	0.00528	0.99834
2.2	12.49487	0.71877	0.25053	0.00502	0.9984
2.4	11.32743	0.65611	0.24891	0.00472	0.99839
2.6	10.404935	0.62762	0.24591	0.00449	0.99842
2.8	9.62864	0.59438	0.24392	0.00428	0.99843
3	8.96001	0.565365	0.24148	0.00409	0.99848
3.5	7.644625	0.510075	0.2373	0.00368	0.99849
4	6.669065	0.46962	0.23107	0.00339	0.9985
4.5	5.930145	0.419135	0.22861	0.00314	0.99834
5	5.303595	0.404005	0.22174	0.00293	0.9986
5.5	4.81337	0.376335	0.21745	0.00274	0.99863
6	4.405535	0.355785	0.21221	0.00257	0.99866
7	3.767385	0.32089	0.20233	0.00228	0.99875
8	3.28895	0.293915	0.19049	0.00203	0.99883
9	2.913665	0.27037	0.17803	0.0018	0.99891
10	2.61863	0.251795	0.16469	0.0016	0.99901
11	2.37502	0.237605	0.14964	0.0014	0.99913
12	2.15815	0.22429	0.13337	0.00118	0.99925
13	1.993605	0.207255	0.12075	9.86837E-4	0.99935
14	1.85211	0.19527	0.10955	7.9535E-4	0.99947
15	1.73336	0.208455	0.1038	6.05195E-4	0.99953
16	1.62278	0.205545	0.09346	4.33936E-4	0.99972
17	1.52792	0.19606	0.09671	2.85155E-4	0.99974
18	1.443685	0.20475	0.10299	1.78292E-4	0.99974
19	1.36834	0.20414	0.11423	1.03344E-4	0.99977
20	1.299265	0.23284	0.10835	6.18734E-5	0.99982
21	1.278405	0.25074	0.128	3.89289E-5	0.99939
22	1.222535	0.292045	0.11103	2.44902E-5	0.99947

Table S4. Best fitted parameters (χ_T, χ_S, τ and α) with the extended Debye model for compound **Dy_2H_2SQ** at 1200 Oe in the temperature range 2.8-22 K.

T / K	χ_T / cm^3 mol^{-1}	χ_S / cm^3 mol^{-1}	α	τ / s	R^2
2.8	10.03878	0.8653	0.34611	5.75021	0.9999
3	9.327755	0.7921	0.33309	4.04408	0.99978
3.5	8.1227	0.474725	0.34053	1.84806	0.99675
4	6.80923	0.44989	0.28567	0.87591	0.99745
4.5	5.96388	0.415025	0.25299	0.48766	0.99769
5	5.292545	0.39337	0.22246	0.29206	0.99848
5.5	4.78208	0.36982	0.201	0.18788	0.99889
6	4.358165	0.34825	0.18196	0.1258	0.99908
7	3.737245	0.31204	0.16171	0.06368	0.99937
8	3.252425	0.283565	0.13779	0.03474	0.99953
9	2.88233	0.26392	0.11846	0.02027	0.99968
10	2.5877	0.2411	0.10715	0.01261	0.99978
11	2.349795	0.226585	0.09388	0.00802	0.99984
12	2.14007	0.21354	0.08538	0.00507	0.99985
13	1.979785	0.202935	0.07831	0.00336	0.99987
14	1.842435	0.201215	0.07481	0.00218	0.99986
15	1.72291	0.194455	0.08076	0.00136	0.99986
16	1.62203	0.189395	0.09955	7.95483E-4	0.99977
17	1.527615	0.201615	0.1158	4.42112E-4	0.9997
18	1.44439	0.192705	0.13726	2.27704E-4	0.99965
19	1.366325	0.202615	0.14104	1.1935E-4	0.99972
20	1.298785	0.259915	0.13007	6.78151E-5	0.9996
21	1.289635	0.299225	0.13702	4.16429E-5	0.99891
22	1.22586	0.37329	0.09225	2.60083E-5	0.99953

Table S5. Computed energy levels (the ground state is set at zero), component values of the Lande factor *g* and wavefunction composition for each m_J state of the ground-state multiplet for [**Dy1HSQ**]$^-$.

KD	Energy (cm^{-1})	g_X	g_Y	g_Z	Wavefunction composition*
1	0.0	0.00	0.00	19.69	0.97 |±15/2>
2	220.3	0.35	0.61	16.29	0.88 |±13/2>
3	278.8	0.12	1.24	17.99	0.53 |±1/2> + 0.32 |±3/2>
4	368.2	5.14	6.65	8.52	0.31 |±3/2> + 0.26 |±11/2> + 0.22 |±1/2> + 0.15 |±5/2>
5	415.7	1.21	2.34	12.43	0.39 |±11/2> + 0.33 |±5/2> + 0.13 |±7/2>
6	447.1	1.57	3.30	9.18	0.37 |±7/2> + 0.27 |±11/2> + 0.14 |±1/2> + 0.11 |±5/2>
7	471.6	0.15	1.07	12.64	0.79 |±9/2>
8	543.6	0.08	0.20	18.67	0.34 |±7/2> + 0.27 |±5/2> + 0.16 |±3/2> + 0.13 |±9/2>

* Only the contributions ≥ 10% are given.

Table S6. Computed energy levels (the ground state is set at zero), component values of the Lande factor *g* and wavefunction composition for each m_J state of the ground-state multiplet for [**Dy2HSQ**]$^-$.

KD	Energy (cm^{-1})	g_X	g_Y	g_Z	Wavefunction composition*
1	0.0	0.00	0.00	19.70	0.97 |±15/2>
2	224.8	0.38	0.73	16.23	0.88 |±13/2>
3	279.1	0.06	1.12	18.08	0.52 |±1/2> + 0.32 |±3/2>
4	377.3	4.86	6.15	7.89	0.33 |±11/2> + 0.28 |±3/2> + 0.17 |±1/2> + 0.13 |±5/2>
5	417.7	1.96	3.11	12.26	0.31 |±11/2> + 0.26 |±5/2> + 0.10 |±7/2> + 0.10 |±3/2> + 0.10 |±9/2>
6	454.8	0.01	3.34	11.64	0.40 |±7/2> + 0.19 |±5/2> + 0.18 |±11/2>
7	488.9	0.76	2.00	13.92	0.61 |±9/2> + 0.11 |±11/2>
8	557.0	0.11	0.28	18.65	0.33 |±7/2> + 0.26 |±5/2> + 0.16 |±3/2> + 0.14 |±9/2> + 0.10 |±1/2>

* Only the contributions ≥ 10% are given.

Table S7. Computed energy levels (the ground state is set at zero), component values of the Lande factor *g* and wavefunction composition for each m_J state of the ground-state multiplet for **DyQ**.

KD	Energy (cm^{-1})	g_X	g_Y	g_Z	Wavefunction composition*
1	0.0	0.07	0.08	18.93	0.89 |±15/2>
2	45.3	0.22	0.43	16.36	0.62 |±13/2> + 0.22 |±11/2>
3	89.0	3.97	4.45	11.50	0.41 |±11/2> + 0.18 |±5/2> + 0.12 |±3/2> + 0.10 |±13/2>
4	117.2	0.68	4.28	13.34	0.50 |±9/2> + 0.18 |±7/2> + 0.11 |±13/2>
5	157.5	1.72	4.59	12.34	0.36 |±7/2> + 0.18 |±3/2> + 0.18 |±5/2>
6	208.5	0.83	1.44	14.75	0.37 |±1/2> + 0.26 |±5/2> + 0.20 |±3/2> + 0.10 |±7/2>
7	241.5	0.21	1.60	16.97	0.44 |±1/2> + 0.28 |±3/2> + 0.10 |±5/2>
8	294.6	0.13	0.45	18.42	0.19 |±11/2> + 0.19 |±5/2> + 0.16 |±3/2> + 0.16 |±9/2> + 0.14 |±7/2> + 0.11 |±13/2>

* Only the contributions ≥ 10% are given.

Table S8. Intermolecular (blue/green) and intramolecular (red) Dy-Dy distances and the corresponding computed dipolar constants for **Dy_2H_2SQ**.

Dy1	J_1	J_2	J_3	J_4	J_5	J_6	J_7	J_8
$d_{Dy\text{-}Dy}$ / Å	16.63	9.98	16.63	11.53	14.29	21.58	10.37	14.29
J / cm^{-1}	0.014	0.255	-0.008	-0.107	-0.021	0.022	0.189	-0.021
Dy2	J_1	J_2	J_3	J_4	J_5	J_6	J_7	J_8
$d_{Dy\text{-}Dy}$ / Å	17.01	9.98	14.19	11.53	17.01	21.58	10.37	14.19
J / cm^{-1}	0.024	0.255	0.039	-0.107	-0.013	0.022	0.189	-0.032

Corresponding color code (Figure S26): $J^{Dy1-Dy1}_{inter}$; $J^{Dy1-Dy2}_{inter}$; $J^{Dy1-Dy2}_{intra}$

Table S9. Intermolecular (blue) and intramolecular (red) Dy-Dy distances and the corresponding computed dipolar constants for **Dy_2Q**.

	J_1	J_2	J_3	J_4	J_5	J_6	J_7	J_8
$d_{Dy\text{-}Dy}$ / Å	6.07	12.62	11.68	12.32	21.65	13.63	13.08	11.68
J / cm^{-1}	-0.650	0.045	-0.049	-0.080	-0.013	0.008	0.097	0.049

Corresponding color code (Figure S27)